International Journal of Control, Automation and Systems 18(12) (2020) 3204-3217
http://dx.doi.org/10.1007/s12555-019-1073-6
ISSN:1598-6446 eISSN:2005-4092
http://www.springer.com/12555

Task Assignment for Deploying Unmanned Aircraft as Decoys

Dileep M V, Beomyeol Yu, Seungkeun Kim*, and Hyondong Oh

Abstract: This paper proposes a task assignment based on auction algorithm for a decoy mission using multiple UAVs which can hover against anti-ship missiles. An optimal deployment direction of decoys are also decided based on the cost function that is calculated with the expected signal power of a seeker and decoy, the distance between them, and fuel availability of the decoys. A simple kinematics is considered to generate two-dimensional motions of anti-ship missiles and a target ship. Numerical simulations are conducted under a visualization environment and validate the performance of the proposed algorithm. A parametric study is also conducted for the decoy mission with multiple missiles and decoys. Lastly, non-linear simulations for ducted fan Unmanned Aerial vehicles (UAVs) are performed to evaluate the feasibility of the proposed high-level task assignment comment for the decoy mission.

Keywords: Auction algorithm, decision making, ducted-fan decoy, task assignment, UAV path planning.

1. INTRODUCTION

Unmanned aerial vehicles have become popular because of their highly autonomous capabilities. Manned vehicles are gradually replaced by unmanned vehicles in various fields like military applications, reconnaissance, surveillance, intruder tracking, and border patrol etc., because of its minimal human requirements and risks. A higher degree of autonomy is needed to achieve a fully autonomous system which can accomplish the challenging mission in an efficient manner [1]. In order to improve the autonomy efficiently, instead of a single system, the inherent redundancy and robustness of multiple systems can be utilized [2].

Cooperation of a large number of small Unmanned Aerial vehicles (UAVs) with autonomous capabilities is called a UAV swarm. It can handle complex missions for existing operational concepts using a large but single UAV could not deal with [3]. The large cardinality of a UAV swarm makes it nearly impossible for humans to guide each of them directly, and thus autonomous decision making is needed. In this sense, cooperative control and decision mechanisms for the UAV swarm have got the attention including task assignment, path planning, and tactical decision making [4, 5]. One of the main challenges for the utilization of a swarm is collective task assignment/decision making [6, 7]. Thus, this paper addresses the task assignment for multiple UAVs as decoys and tackles the defence against anti-ship missiles (ASMs) in a maritime mission as an example scenario. The purpose of multi UAV task assignment is to allocate necessary tasks to UAVs, so as to maximise the performance of the mission. Here, the task is to allocate optimum number of decoys against each ASMs to enhance protection of the friendly ship, and the result of task assignment directly determined how well the missions were performed. The task assignment proposed in this study can be extended to other types of unmanned aircraft deployment by modifying a cost function and the related scenario [8].

Since the decoy application is based on a maritime mission, vertical take-off and landing (VTOL) UAVs have advantages on it, considering the limited area in the ship deck to operate aerial platforms and their hovering capabilities [9]. The decoy mission is known to be the most effective way for a ship to survive from ASM in a battle field [10]. An ASM can be launched from a variety of systems such as fighter jets, naval ships and land bases etc [11]. Due to the small radar cross section (RCS) of ASMs in sea clutter, it is difficult to find an ASM to a defense ship before a terminal phase [12]. Various topics for the decoy missions against ASMs have been widely studied due to this importance. Decoy systems are mainly classified into two: a towed type [13] and a mobile type. In towed types, a decoy is basically linked with a target ship or an aircraft. Protection of an aircraft from radio frequency (RF) missile attack is discussed in [14] and a part of this is also

Manuscript received December 25, 2019; revised May 28, 2020; accepted June 25, 2020. Recommended by Associate Editor Son-Cheol Yu under the direction of Editor Chan Gook Park. This research was supported by a grant to Bio-Mimetic Robot Research Center Funded by Defense Acquisition Program Administration, and by Agency for Defense Development (UD130070ID).

Dileep M V, Beomyeol Yu, and Seungkeun Kim are with the Department of Aerospace Engineering, Chungnam National University, Daejeon 34134, Korea (e-mails: dileeppsla@gmail.com, yubeomyeol@gmail.com and skim78@cnu.ac.kr). Hyondong Oh is with the School of Mechanical, Aerospace and Nuclear Engineering, Ulsan National Institute of Science and Technology, Ulsan 44919, Korea (e-mail: h.oh@unist.ac.kr).
* Corresponding author.

included to the current work. Comprehensive study based on towed radar active decoys (TRAD) to defend against a mono-pulse radar has been carried out in [15]. However, towed types have the limitation of operation regions and it might degrade the maneuverability of a target ship or aircraft. To address this issue, mobile types have been investigated in [16–18] and has better performance compared to towed types.

Mobile type decoys require advanced technologies to make them moving with decoy devices. The deployment process has been investigated in [16], by considering distance, deployment angle and required gains/powers. The work proposes an optimal deployment parameters to distract the ASM. Vermeulen and Maes [17] discussed an analytical derivation of the miss distance at intercept to the target with the seeker. Interceptors are utilized for a mobile decoy [18] for cooperative mission and is discussed in [19] and has better performance compared to others. A cooperative air defense process using a ship-to-air missile (SAM) is discussed in [20] for a single attach.

As mentioned earlier, nowadays many researchers are focusing on task assignment for multi-agent systems to improve the efficiency of cooperate missions [21]. Yoo *et al*. [22] considered heterogeneous UAVs to assign the optimal number to an integrated air defense system for a suppression of enemy air defence (SEAD) mission. A probability based resource management algorithm is performed to do the allocation of UAVs with out TA. A new task assignment algorithm is proposed by Jia *et al*. [23] for cooperative multi-UAV task assignment problem and it is formulated as a combinatorial optimization problem, and solved by modified genetic algorithm and path elongation algorithm.

In this study, the mission response times and the launch directions of decoys are the critical parameters that can determine the success/failure of the mission. Auction algorithm is chosen for the task assignment because of its higher computation speed compared to other optimization techniques [24]. Based on the above literatures, this paper proposes a task assignment algorithm based on an auction algorithm with a minimum-number-of-UAV requirement for multi-decoy deployment to protect a friendly ship from ASMs. The cost function is formulated by considering the expected signal power of a seeker and a decoy, the distance between them, and fuel availability of the decoys. Based on the cost value, the auction algorithm will allocate the decoys to the particular ASM by satisfying minimum requirements. The term minimum requirement indicate the minimum number of decoys/agent required to perform each task in a risk free manner.

The optimal deployment direction of UAVs with mobile jammer are also included to distract multiple ASMs. When the ship detects the ASMs, the task assignment procedure will be carried out, and assigned decoys will move towards optimal directions to distract the ASMs from the ship. Decoys are attractive because they provide a source of radiation that can capture the radar seeker and direct the missile away from the ship. The decoys are only sources of radar jamming and there is a chance of distroy decoy by the missile. Thus return back policy for the decoys are not included in the system. To simulate this decoy mission, a 2D point mass model is used for multiple ASMs and a target ship [10]. Each ASM model uses a guidance law using a proportional navigation guidance (PNG) law for realistic simulations. Additionally, this paper proposes the deployment strategy of the decoys by considering the expected signal power (ESP) between multiple seekers and decoys. Thus, this paper evaluates the protection provided by active off-board decoys which are deployed by ships during an engagement against a radar guided ASM. Parametric study has been done to evaluate the performance of task assignment process.

The rest of this paper is organized as follows: Section 2 explains the models used to study the decoy mission: a ship model, a ship-missile engagement model, a decoy dynamic model and the signal models for seekers and decoys. Section 3 describes the mission scenario for the deployment of decoys and an optimal direction strategy. Section 4 proposes the task assignment process where the cost function and the auction-based algorithm are explained. In Section 5, 2D simulation along with parametric study and a six degree-of-freedom simulations with ducted-fan UAV dynamics are given to verify the feasibility of the proposed task assignment. Finally, the paper is concluded in Section 6.

2. PROBLEM DEFINITION

In order to accomplish the decoy mission against ASMs using task assignment, it is necessary to describe a ship model, a ship-missile engagement model, decoy dynamic model and the signal model for seeker and a decoy. Basically the missile seeker always tends towards the centre of gravity of the target source. So in addition to the above models, a proportional navigation guidance (PNG) law is applied to the ASM guidance. The key of the mission is how unmanned aircraft used as decoys protect the ship from ASMs with safe distances.

2.1. Target ship kinematics model

The section describes the point mass model for target ship kinematics with zero or negligible velocity in the direction perpendicular to heading [25].

$$\begin{bmatrix} \dot{X}_s \\ \dot{Y}_s \\ \dot{\varphi}_s \end{bmatrix} = \begin{bmatrix} V_s \cos\varphi_s \\ V_s \sin\varphi_s \\ \omega_s \end{bmatrix}, \tag{1}$$

where (X_s, Y_s) are the Cartesian coordinates of the ship, φ_s is the heading angle, V_s is the speed in the (x, y) plane, and ω_s is the turning rate of the ship.

2.2. Anti-ship missile model

In this paper, the anti-ship missile model is derived by considering some assumptions as follows. 1) a point mass model is adopted for the missile; 2) initially the missile maintains a constant altitude for sea-skimming maneuver; 3) the missile velocity is constant. The 2D kinematics equation to represent an ASM model [10] is given by

$$\dot{X}_{m,j} = V_{m,j}\cos\varphi_{m,j}, \tag{2}$$
$$\dot{Y}_{m,j} = V_{m,j}\sin\varphi_{m,j}, \tag{3}$$

where j is the index of the missile, $X_{m,j}$ and $Y_{m,j}$ are the positions of the missiles in the inertial frame. $V_{m,j}$ and $\varphi_{m,j}$ denote the velocity and heading angle of the ASM, respectively.

This study concentrates on a missile's terminal guidance phase; thus, it is assumed that its target information is known to the missile, guidance law is applied based on a missile engagement model. Fig. 1 shows the geometry of the missile engagement model. Proportional navigation guidance (PNG) is applied that as [16]

$$a_{c,j} = N' V_{c,j}\dot{\lambda}_j, \tag{4}$$

where $a_{c,j}$ is an acceleration command, N' is a constant design factor that is usually determined between three and five, $V_{c,j}$ denotes a missile-target closing velocity, and λ_j is a line-of-sight (LOS) angle. The closing velocity is defined as

$$V_{c,j} = \dot{R}_{s,j} = V_s - V_{m,j}, \tag{5}$$

where $R_{s,j}$ is the relative distance between the j^{th} missile and the target ship. The LOS angle can be calculated as

$$\lambda_j = \tan^{-1}\left(\frac{Y_s - Y_{m,j}}{X_s - X_{m,j}}\right). \tag{6}$$

Differentiating the above equation with respect to time yields

$$\dot{\lambda}_j = \left(\frac{X_{r,j}\dot{Y}_{r,j} - Y_{r,j}\dot{X}_{r,j}}{R_{s,j}^2}\right), \tag{7}$$

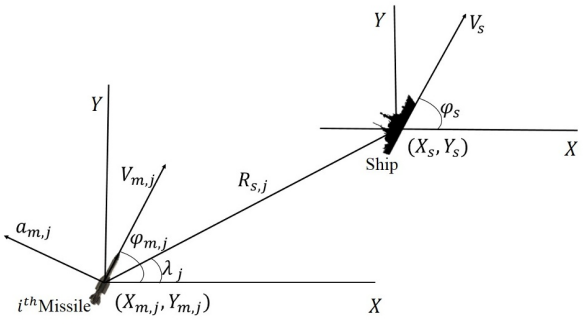

Fig. 1. Geometry of missile-target engagement.

where $X_{r,j}$ and $Y_{r,j}$ indicate the relative positions between the target from the j^{th} missile. This can be simplified as

$$\dot{\lambda}_j = \frac{V_{m,j}}{R_{s,j}}\sin(\lambda_j - \varphi_{m,j}) + V_s\sin(\lambda_j - \varphi_s). \tag{8}$$

The heading angle command of the missile is defined as follows:

$$\dot{\varphi}_{m,j} = \frac{a_{m,j}}{V_{m,j}} = a_{c,j} = N' V_{c,j}\dot{\lambda}_j, \tag{9}$$

where $a_{m,j}$ indicates the lateral acceleration of the j^{th} missile. The missile-target closing velocity is derived as

$$V_{c,j} = V_{m,j}\cos(\lambda_j - \varphi_{m_j}) + V_s\cos(\lambda_j - \varphi_s). \tag{10}$$

Generally, anti-ship missiles will be equipped with an active radio frequency seeker, which is perceived as a very effective way to track moving targets. Identification of the target is based on the reflected radar signal from the ship to the missile seeker. The back scattered signal to the seeker is represented as [16]

$$S_j = P_j G_{t,j} G_{r,j} \Lambda_j^2 \sigma / (4\pi)^3 R_{s,j}^4, \tag{11}$$

where P_j is the j^{th} seeker output power, and $G_{t,j}$ and $G_{r,j}$ are the transmitting and receiving antenna gains of the j^{th} seeker, respectively. Λ_j is the wavelength of the j^{th} seeker, and σ is equal to the radar cross section (RCS) of the target ship.

2.3. Decoy model

The point mass model is considered for decoys. The non-linear kinematic model [25] of a decoy with zero velocity in the direction perpendicular to the heading is given by

$$\begin{bmatrix}\dot{X}_{d,i}\\ \dot{Y}_{d,i}\\ \dot{\varphi}_{d,i}\end{bmatrix} = \begin{bmatrix}V_{d,i}\cos\varphi_{d,i}\\ V_{d,i}\sin\varphi_{d,i}\\ \omega_{d,i}\end{bmatrix}, \tag{12}$$

where i is the index of a decoy, and $X_{d,i}$ & $Y_{d,i}$ are the Cartesian coordinates of the decoy, $\varphi_{d,i}$ is the heading angle, $V_{d,i}$ is the velocity in the (x,y) plane, $\omega_{d,i}$ is the turning rate of the decoy.

Each decoy is equipped with a omnidirectional signal jammer. It amplifies and emits a repetitive delay signal that is larger than the reflected signal of the target trap to the missile. Thus, the decoy distracts missiles from the ship. The decoy signal can be calculated as [16]

$$J_{i,j} = P_{d,i} G_{d,i} G_{r,j} \Lambda_j^2 / (4\pi)^2 R_{i,j}^2, \tag{13}$$

where $P_{d,i}$ is i^{th} decoy's jammer output power, $G_{d,i}$ is the transmitting antenna gain of i^{th} decoy's jammer, and $R_{i,j}$ is the distance between the j^{th} seeker and i^{th} decoy.

3. GENERAL MISSION SCENARIO

This section explains the general scenario for protection of friendly ship against anti-ship missile. Generally, anti-ship missile attack has four steps. 1) target acquisition, 2) target tracking, 3) mid-course guidance, and 4) terminal guidance [11, 16]. From here onwards, the words ASM and missile will be used interchangeably. In this paper, we consider only the terminal guidance phase and assume that the missile seeker is already on and it is in a lock-on tracking mode. Additionally, because the seeker's transmission provides a clear threat signature to the target ship, the later the seeker turns on, the shorter reaction time available for the target ship [16].

Fig. 2 shows the anti-ship missile attack procedure. As a defending side, there is a chance to interrupt the missile engagement procedure by deploying active decoys. Since it is assumed that the electronic supporting measures (ESM) has longer detection ranges than the attacker's radars; immediately after decoy deployment, the missile does not see either the ship or the decoy [12]. Based on the signal strength, the missile receives higher power signals from the decoys other than the target ship. Thus, missiles start tracking the decoys by considering them as real targets. While the missiles are maneuvering, the ship will be given time to escape or take advantages against the missile.

Main concentration of this study is the effective deployment of decoys against the missile based on their preferences. Initially, the decoys are in a circular formation around the ship to improve safety precautions. When the ship senses the missiles, it will perform a task allocation for each decoy. The details about the task assignment can be found out from the coming section. After this task allocation steps, way point commands will be sent to each decoy by path planning. Fig. 3 shows the ship response and missile defense procedure.

In order to provide active protection, the distance between the ship and decoys should be as far as possible, so that the probability of the seeker locking back on the ship is small. During this process, the decoys should not move so far away that it exceeds the seeker beam widths and causes out of sight for the seeker. As an optimal deployment angle based on [16], the decoys move towards the perpendicular direction of the line of sight (LOS) between the ASM and the ship with a maximum flight speed to distract the missiles. Fig. 4 shows the geometry of a single decoy deployment for a single missile, where R_d is the distance between the decoy and the ship. At the time of detection, the decoy heading angle, $\varphi_{d,i}$ is updated as

$$\varphi_{d,i} = \begin{cases} \varphi_{d_0,i}, & 0 < t < t_{det}, \\ \varphi_{det,i}, & t_{det} \le t \le t_{max}, \end{cases} \tag{14}$$

where t_{det} and t_{max} are defined as the missile detection time and total time of flight in the mission, $\varphi_{d_0,i}$ indicates the UAV heading angle which is same as ship's heading and $\varphi_{det,i}$ is the i^{th} decoy heading angle after the missile detection as

$$\varphi_{det,i} = \begin{cases} \varphi_{d,i} + (\varphi_{m,j} + \pi/2), & 0 \le \lambda_j \le \pi, \\ \varphi_{d,i} + (\varphi_{m,j} - \pi/2), & \pi < \lambda_j < 2\pi. \end{cases} \tag{15}$$

Fig. 5 shows the entire process performed by individual components in the mission scenario.

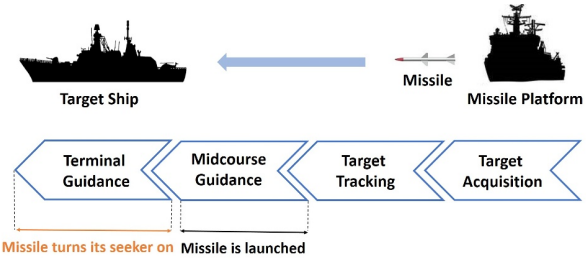

Fig. 2. Anti-ship missile attack procedure.

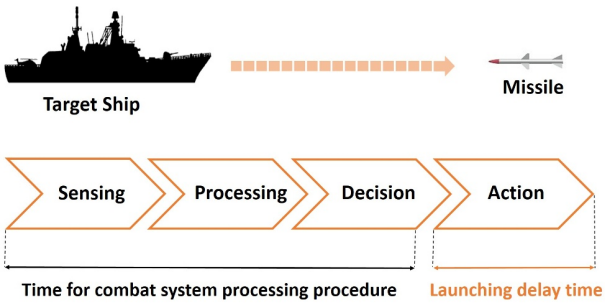

Fig. 3. Ship response and missile defence procedure.

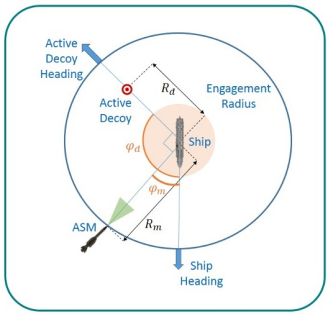

Fig. 4. Decoy deployment scenario.

4. TASK ASSIGNMENT

Task assignment (TA) is necessary to distribute or assign the task for individuals based on required criteria. Tasks can be expressed as the set of lower level goals

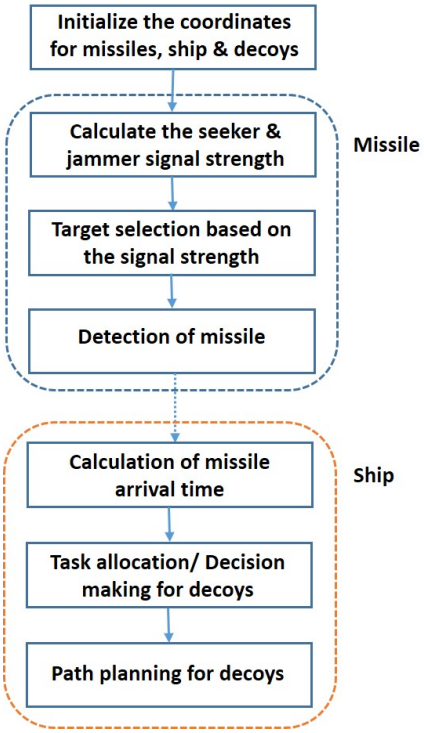

Fig. 5. Decoy deployment scenario.

necessary for achieving the overall mission goal [27]. In this study, the optimal allocation of UAVs to each missile, as decoys to protect a friendly ship is considered as task. Because the response time is very limited in this problem, the proposed TA method should produce a valid solution within a reasonable time for real-time application. In addition, this algorithm is an event trigger-based process [28, 29], which means that the algorithm will work when the target ship detects a missile. Detailed explanation of the algorithm can be find out in the following sections.

4.1. Cost function

In order to achieve the maximum protection of a ship, optimal allocation of decoys against missiles has to be done based on the ship and missile engagement model. It is assumed that, if the ship detects a missile, it will increase alert capability and will get the information about other missiles by the help of sensing information sources. Thus, at the time of first missile detection, the time of arrival of all the missiles can be estimated assuming salvo attack as

$$t_{s,j} = \frac{R_{s,j}}{V_{m,j}}, \tag{16}$$

where $R_{s,j}$ denotes the relative distance between the j^{th} missile and the target ship, and $V_{m,j}$ is the velocity of the j^{th} missile.

The relative distance between each decoy and the missile is calculated as

$$R_{i,j} = \sqrt{(X_{d,i} - X_{m,j})^2 - (Y_{d,i} - Y_{m,j})^2} \tag{17}$$

where $(X_{d,i}, Y_{d,i})$ and $(X_{m,j}, Y_{m,j})$ denotes the coordinates of the decoy and missile in the Cartesian plane, and i and j denote the indices of the decoy and missile, respectively.

As mentioned above the task assignment process in this mission is an event triggering-based process, the cost function considers the static information at the time of triggering. Thus, cost function for TA is be formulated based on time of arrival, relative distance between decoy and missile, and signal strength of the seeker. The cost function is defined as

$$C_{i,j} = \hat{R}_{i,j}/\hat{e}_i + \hat{t}_{s,j} + \hat{J}_{i,j}, \tag{18}$$

where $\hat{R}_{i,j}$ and $\hat{J}_{i,j}$ indicate the normalized values of the relative distance between the j^{th} missile and the i^{th} decoy, and jammer signal strength for the j^{th} missile and the i^{th} decoy, respectively. In addition to the above mentioned terms, a fuel/energy term is also considered. $\hat{e}_i$ indicates the normalized value of the remaining fuel for i^{th} decoy at the time of missile detection.

The cost function is developed such a way that it should consider the effect of expected signal power of a seeker and decoy, the distance between them, and fuel availability of the decoys. From (18), the first term indicates the relative distance between the friendly ship with each UAV based on their battery power at the time of an ASM detection. Second and third term indicates the time of arrival of the each missile and the decoy gamer signal respectively. Based on this calculation, the overall weight-age to be given to each UAV will be known and it is distributed based on auction algorithm.

4.2. Auction based task assignment

An auction is a process of assigning a set of goods or services to a set of bidders according to their bids and the auction criteria. In this paper each ship/central unit works as a auctioneer will receive all decoys costs which are sent as bids. The task can be allotted to the decoy with minimum cost/bid and repeat the process for all tasks [25, 26].

Consider a set of n_q tasks, $Q = \{q_1, ..., q_{n_q}\}$ and a set of n_a agents, $A = \{a_1, ..., a_{n_a}\}$. For each task q_j, each agent a_i is associated with a different work capacity that is expressed as a form of cost function in the previous section where $i = 1, 2, ..., n_a$ and $j = 1, 2, ..., n_q$. A minimum requirement in terms of the minimum number of agent participation per task is expressed as $n_{g_j} \geq n_{g_{min}}$ where n_{g_j} and $n_{g_{min}}$ are the number of agents in the group, g_j and the minimum number of agents required to perform the task q_j, respectively. Note that the product of the total number of tasks and the minimum agents required to perform the task should be less than or equal to the total number of agents, i.e., $n_{g_{min}} n_q \leq n_a$. Here, n_q, n_a, n_{g_i}, and $n_{g_{min}}$ are non-negative.

Algorithm 1: Task assignment algorithm.

input : Cost function $C_{i,j}$ where $i \in \{1,2,.....n_a\}$ and $j \in \{1,2,.....n_q\}$
output: Agent allocations to each task

for $k_1 \leftarrow 1$ **to** n_q **do**
  if $n_{g_j} \leq n_{g_{min}}$ **then**
    Find $H_c = min\, C_{i,:}$.
    Assign the i^{th} agent to the task with cost H_c and update g_i.
    Remove the i^{th} agent from the group.
    if $n_{g_l} = n_{g_{min}}, l \in i$ **then**
      Eliminate the group, g_l from the assigning process.
      Find $G_c = min\, C_{:,j}$.
      Assign the agent with cost G_c to j^{th} task and update g_i.
      Eliminate the group are satisfying $n_{g_j} = n_{g_{min}}$.
      if $n_{g:} = n_{g_{min}}$ **then**
        break

for $k_2 \leftarrow jn_{g_{min}}$ **to** n_q **do**
  Find $K_c = min\, C_{i,:}$.
  Assign the i^{th} agent to the task with cost K_c and update g_i.

This study proposes the task assignment (TA) based on an auction algorithm [30] to satisfy scalability and real-time application. The initial stage of the task allocation algorithm works based only on cost from (18) and the agent can be allocated to the task having the lowest cost. Then the TA calculates the cost for each agent with respect to each task using (18) with initializing as $n_{g_j} = 0$. After that, the number of agents assigned to each group, n_{g_j} will be updated. When $n_{g_j} = n_{g_{min}}$, the agent allocation for the particular group, g_j will be stopped, and the auction algorithm will be applied for the other tasks in the same way. This process will be continued for every task; then, Q will be occupied by the minimum number of agents. After this the TA will continue with the auction procedure. The auction-based task assignment algorithm is expressed as a pseudo code in Algorithm 1. In this study a task assignment algorithm ia applied for multi-decoy deployment process to protect a friendly ship from an ASM and minimum requirement is also considered as minimum-number-of-decoys per task.

5. NUMERICAL SIMULATION AND DISCUSSION

In this section, the first part explains a simulation example performed to evaluate the decoy mission using multiple anti-ship missiles and mobile decoys. Since we use only simple kinematics for this study, it is necessary to verify the real-time response of the decoys when the task assignment gives the commands to the inner loop. Thus in second part, we adopt ducted-fan UAVs as mobile decoys that have VTOL capability and easy/safe operability because their shrouds cover propellers for 6-DOF dynamic simulations.

5.1. Example simulation for decoy deployment against anti-ship missiles

In this example, the number of missiles, n_m are considered as three and the number of decoys, n_d as 20. The minimum number of decoys per task is defined as, $n_{g_{min}} = 3$. A friendly ship is moving with a constant velocity, $V_s = 15m/s$ and heading angle, $\varphi_s = 0deg$. Initial coordinates of the ship is chosen as $(X_{s_0}, Y_{s_0}) = (0,0)$. The simulation is carried out for 100 seconds. Initial conditions of the missiles are shown in Table 1.

Initially, the decoys are distributed in a circular formation with a radius $R_{sep} = 130m$ around the ship center and keep moving along with the ship by following the ship's velocity and heading angle. The initial position of the i^{th} decoy is expressed as

$$\begin{cases} X_{d_0,i} = X_{s_0} + R_{sep}\cos\beta_i, \\ Y_{d_0,i} = Y_{s_0} + R_{sep}\sin\beta_i, \end{cases}$$

where β_i is the orientation of the decoy with respect to the center of the ship. For the i^{th} decoy,

$$\beta_i = 2\pi i/n_a. \tag{19}$$

The remaining fuel level of the decoy is assumed to be as the linearly increasing with its index as given by

$$e_i = e_{min} + \left(\frac{e_{max} - e_{min}}{n_a}\right) i, \tag{20}$$

where e_{min} and e_{max} are the maximum and minimum values required for the decoys. In this paper, we use $e_{min} = 85\%$ and $e_{max} = 100\%$.

The multiple missile seekers and decoy repeaters assume the same models, and the signal parameters are taken from [16] as shown in Table 2. For convenience, the signal strength calculations of seekers and jammers have been converted into log scale (dBm). Thus, (11) and (13) can be rewritten as

$$S_j = 10logP_{k,j} + G_{t,j} + G_{r,j} + 10log\sigma - 40logR_{s,j}$$

Table 1. Missile initial conditions.

Parameters	M_1	M_2	M_3	Unit
X_{m_0}	20,000	5,000	-10,000	m
Y_{m_0}	20,000	20,000	20,000	m
V_{m_0}	350	300	330	m/s
φ_{m_0}	230	300	270	deg

Table 2. Seeker/decoy signal parameters.

Parameters	Values	Units
P_k	200	kw
G_t	35	dB
G_r	35	dB
Λ	0.003	m
σ	50	m^2
P_d	1	kW
G_d	35	dB

$$-20logF_j - 163.4, \tag{21}$$

$$J_{i,j} = 10logP_{d,j} + G_{d,j} + G_{r,j} - 20logR_{i,j} - 20logF_j - 92.45, \tag{22}$$

where F_j is the frequency of the j^{th} seeker signal [16], and its wave length is represented by

$$\Lambda_j = c/F_j, \tag{23}$$

where c denoted as the speed of light in vacuum (3×10^8 m/s). Based on the above mentioned models, the upcoming simulations are performed.

In order to improve the signal strength in a decoy group, a formation strategy is applied, and this will reduce the distance between individual decoys in the group. This is accomplished by altering the heading angle of each decoy after some relaxation time. The relaxation time will reduce the probability of potential collisions while building decoy formation. Equation (14) can be modified as

$$\varphi_{d,i} = \varphi_d + \theta_{d_f,i}, \tag{24}$$

where $\theta_{d_f,i}$ is the formation angle for each decoy and is defined as

$$\theta_{d_f,i} = \tan^{-1}\left(\frac{cg_{j,y} - Y_{d,h}}{cg_{j,x} - X_{d,h}}\right), \tag{25}$$

where $X_{d,h}$ and $Y_{d,h}$ are x and y coordinates of the h^{th} decoy, h is the decoy's index, which are allocated for j^{th} task. $cg_{j,y}$ and $cg_{j,x}$ are the coordinates of the extended centroid for the decoy groups, which are allocated for j^{th} task.

Fig. 6 shows the trajectories of the decoys for the entire mission. The symbol '$\times$' and 'o' indicate the decoy initial and final positions. Initially the decoys are following the ship using a circular formation and it is deviating after TA comment. From figure, it is clear that all the missiles are deviating from the ships and getting attracted by the decoys. Thus, the safety of the ship is ensured by increasing the distance between the ship and missiles. Based on the task assignment in the simulation, among 20 decoys, three are allocated to the first missile, five are allocated to the second missile, and the rest 12 are allocated to the third missile. Each group of decoys flies to the perpendicular direction of its LOS between each missile; thus the

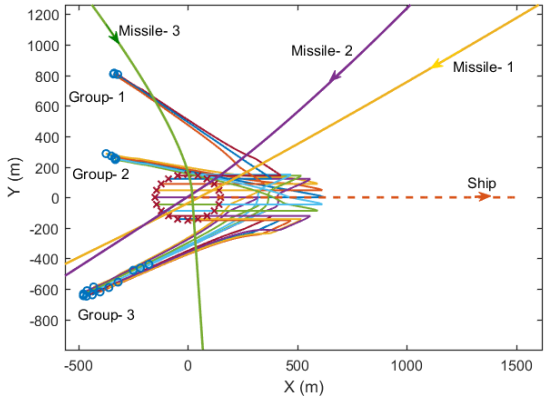

Fig. 6. Decoy trajectories.

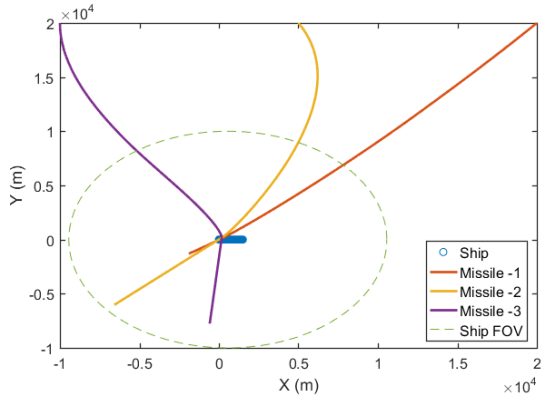

Fig. 7. Ship and missile trajectories.

ship can be survived from the missile attack. Group-1, 2 and 3 are the groups of decoys which are assigned for the missiles 1, 2 and 3, respectively.

Fig. 7 shows the trajectories of the ship and the missiles in the entire simulation time. When the first missile is detected, the ship expands its field of view and detects the other missiles and performs a task assignment based on the pre-described cost. At the time of detection, the decoys will activate their jammer signal generators. This results the missiles trajectory deviation towards the ship and lock-on modes with the decoys.

Fig. 8 shows the relative distances between the ship and missiles along with a safe distance, $d_{safe} = 150$ m. It clearly shows that the relative distance is always less than the safe distance for given parameters; thus, the ship is in a safe condition and ensures maximum protection.

Fig. 9 shows the relative distances among the decoys. This makes it clear that there are no potential collisions during the flight. The minimum distance to avoid collisions among the decoys is set to be 5 m which is shown as a dashed line in Fig. 9. It can be seen that the distance between each decoys are constant during the initial times and is varying after the TA. Fig. 10 illustrates the jammer

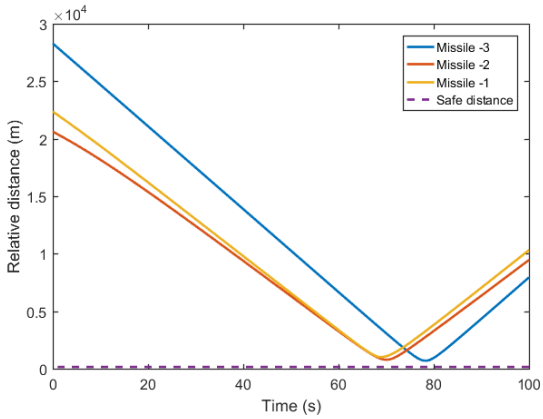

Fig. 8. Relative distances between the ship and the missiles.

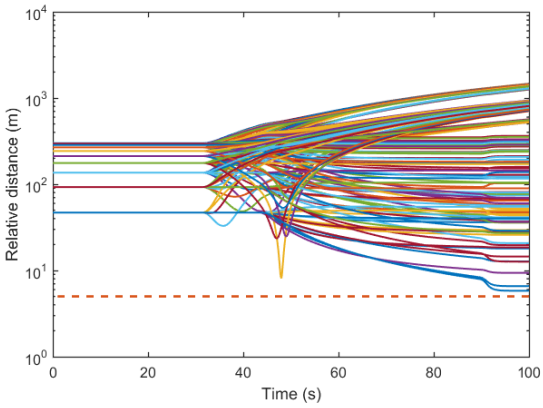

Fig. 9. Relative distances between the decoys.

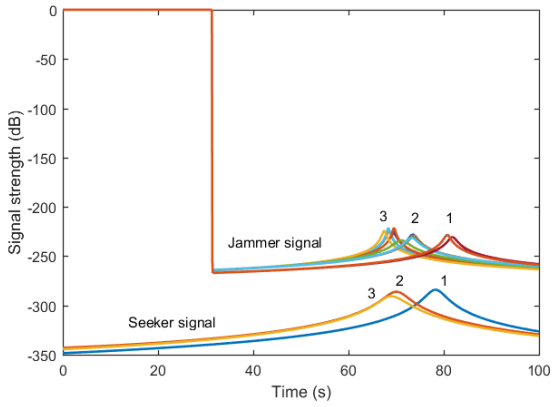

Fig. 10. Jammer and seeker signal strengths.

and seeker signal strengths of the individuals. When the ship detects the first missile at the time, $t = 31.5$ s, the task assignment can be done, and the jammer signal generation starts. In Fig. 10, the number 1, 2, and 3 indicate that the missile indices. After the detection, the jammer signal power is always higher than the seeker; therefore, decoy mission is successful against anti-ship missiles. Because the seeker will always follow the signal which has higher signal strength.

5.2. Parametric study regarding velocity and decision radius.

In order to analyze the performance of the proposed task assignment, a parametric study has been done. Three parameters are considered in this study: 1) decoy velocity; 2) decision radius; 3) missile velocity. The decision radius is the minimum relative distance between the target ship and the missile. An additional uncertainty factor has been added to the performance of the decoys because of meteorological effects, malfunctioning, or missile's anti-counter measures. Thus, the performances of the decoys have been limited to $70\% - 100\%$ and assigned randomly for each decoy in the simulations. The mission success rate is calculated based on the kill distance that is defined as the minimum distance between the ship and the missiles to keep the ship safe. This study considers the kill distance as $R_{kill} = 150$ m.

Table 3 shows the dependency of the decision radius on the success rate of the mission for a maximum velocity of decoy, $V_{d,max} = 15$ m/s. From Table 3, it can be seen that the decision radius has a significant role on the success rate of the mission. As the decision radius increases, the mission success rate also increases. The decoy allocation is also different with respect to the decision radius. Table 4 shows the dependency of maximum decoy velocity on the success rate of the mission for a decision radius, $R_{dec} = 5000$ m. It can be observed that there is a particular threshold for the decoy velocity to get the maximum success rate of the mission.

Fig. 11 presents the success rate of the mission for different decision radii and maximum decoy velocities. It can be seen that, the sudden drop in success rate at decision radii 4000 m because one group of decoys are failing to separate the ASM from the ship at the a distance of 150 m.

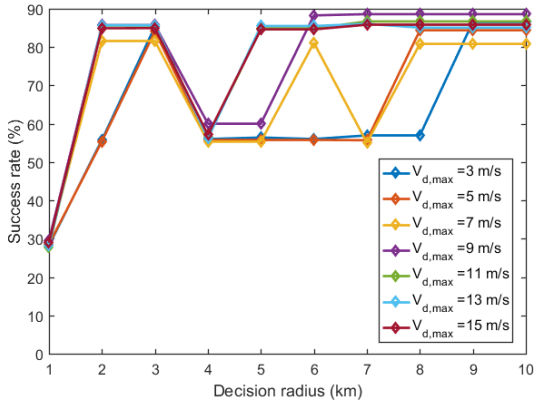

Fig. 11. Succes rate of the mission with respect to decision radius and decoy velocity.

Table 3. Effect of a decision radius on the success rate of the mission.

Decision radius (m)	Decoy allocation			Min. relative distance to the ship (m)			Success rate (%)
	M_1	M_2	M_3	M_1	M_2	M_3	
1,000	3	5	12	2.3	7.7	896.7	28.24
2,000	3	5	12	960.5	789.7	861.6	57.34
3,000	3	5	12	821.1	241.1	829	82.67
4,000	3	4	13	772.1	41.8	805.4	57.67
5,000	3	4	13	751.1	198.1	758	84.84
6,000	3	4	13	746.9	379.7	770	84.84
7,000	3	5	12	732.8	432.7	753.3	85.24
8,000	3	5	12	730.2	574.8	740.1	85.24
9,000	3	5	12	735.6	697.3	727.3	85.24
10,000	3	5	12	745.9	802.4	715.1	85.24

Table 4. Effect of a decoy velocity on the success rate of the mission.

Max. decoy velocity (m/s)	Min. relative distance to the ship (m)			Success rate (%)
	M_1	M_2	M_3	
3	730	128.6	826.4	56.32
5	737.6	16.69	814.3	56.32
7	755.9	93.9	803.8	56.32
9	755	129	794.7	56.32
11	754.6	178	787.8	84.84
13	755.2	196.8	787	84.84
15	751.1	198.1	786.7	84.84

Thus it is observed that the combination of higher decoy velocity ($>$ 9 m/s) and the larger decision radius ($>$ 5000 m) has the maximum success rate.

The effect of missile velocity and decision radius to the mission success is analyzed as shown in Table 5. For this analysis, an assumption has been made that all the missiles have the same velocities under a transonic range. It is observed that the higher decision radius can increase the mission success rate, and the higher missile velocity can reduce the success rate of the mission. Fig. 12 shows the success rate of the mission for different combinations of decision radii and missile velocities.

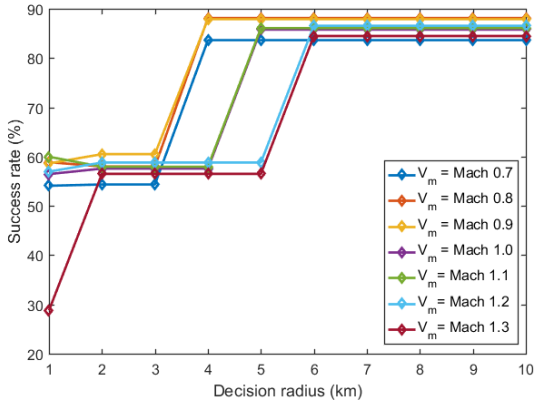

Fig. 12. Success rate of the mission with respect to decision radius and missile velocity.

5.3. Validation of decoy maneuverability using a 6-DOF ducted fan simulation

Lastly, non-linear simulations for ducted-fan UAVs with a decoy mission is performed to evaluate the feasibility of the proposed high-level task assignmnet command. A numerical model of the ducted fan system was introduced using the Newton-Euler method in [31]. This paper briefly revisits the numerical model composed of kinematics and dynamics in the inertial (I) and body (B) frames. Kinematic equations, for translational and rotational motions are expressed as

$$\dot{\boldsymbol{P}} = R_B^I(\phi,\theta,\psi)\boldsymbol{v}, \tag{26}$$

$$\dot{\boldsymbol{\xi}} = H(\phi,\theta)\boldsymbol{\omega}, \tag{27}$$

where $\mathbf{P} = [X,Y,Z]^T$ are positions in the inertial frame, and $\mathbf{v} = [u,v,w]^T$ are velocities in the body frame. Euler angles and angular rates denote $\boldsymbol{\xi} = [\phi,\theta,\psi]^T$ and $\boldsymbol{\omega} = [p,q,r]^T$. R_B^I represents the rotational matrix from the body frame B to the inertia frame I. H denotes a transformation matrix for the Euler rates in terms of the body

Table 5. Effect of a decoy velocity on the success rate of the mission.

Decision radius (m) \ Missile velocity (Mach)	0.7	0.8	0.9	1.0	1.1	1.2	1.3
1,000	54.08	58.86	58.62	56.45	59.97	56.95	28.76
2,000	54.35	58.00	60.50	57.57	57.94	58.80	56.50
3,000	54.35	58.00	60.50	57.57	57.94	58.80	56.50
4,000	83.63	88.11	87.90	57.57	57.94	58.80	56.50
5,000	83.63	88.11	87.90	85.78	86.08	58.80	56.50
6,000	83.63	88.11	87.90	85.78	86.08	86.56	84.47
7,000	83.63	88.11	87.90	85.78	86.08	86.56	84.47
8,000	83.63	88.11	87.90	85.78	86.08	86.56	84.47
9,000	83.63	88.11	87.90	85.78	86.08	86.56	84.47
10,000	83.63	88.11	87.90	85.78	86.08	86.56	84.47

angular velocities [10]. The dynamic model of a single ducted-fan is given as

$$\begin{bmatrix} mI_3 & 0 \\ 0 & \mathbf{J} \end{bmatrix} \begin{bmatrix} \dot{\boldsymbol{v}} \\ \dot{\boldsymbol{\omega}} \end{bmatrix} + \begin{bmatrix} \boldsymbol{\omega} \times m\boldsymbol{v} \\ \boldsymbol{\omega} \times \mathbf{J}\boldsymbol{\omega} \end{bmatrix} = \begin{bmatrix} \boldsymbol{F} \\ \boldsymbol{M} \end{bmatrix}, \tag{28}$$

where m and j denotes the mass and inertial matrices, and $\boldsymbol{F} = [F_x, F_y, F_z]^T$ and $\boldsymbol{M} = [M_x, M_X, M_z]^T$ indicate the external force and moment about the body frame.

A conventional ducted fan configuration includes a fuselage, a propulsion system, a duct, and multiple control flaps [32,33]. Also, gravitational and gyroscopic elements are considered for this terms. The fuselage takes the role of a payload bay, which is equipped with batteries, flight control avionics and so on. The propulsion system includes a rotor system with a stator for an anti-torque structure. The external force and moments for the ducted fan is given by

$$\boldsymbol{F} = \boldsymbol{F}_{fuse} + \boldsymbol{F}_{prop} + \boldsymbol{F}_{duct} + \boldsymbol{F}_{flap} + \boldsymbol{F}_{grav}, \tag{29}$$

$$\boldsymbol{M} = \boldsymbol{M}_{fuse} + \boldsymbol{M}_{prop} + \boldsymbol{M}_{duct} + \boldsymbol{M}_{flap} + \boldsymbol{M}_{gyro}, \tag{30}$$

where $\boldsymbol{F}_{fuse}$, $\boldsymbol{F}_{prop}$, $\boldsymbol{F}_{duct}$, $\boldsymbol{F}_{flap}$, and $\boldsymbol{F}_{grav}$ are denoted as force component in ducted-fan due to fuselage, propulsion system, duct, flaps and gravitation respectively. Similarly, $\boldsymbol{M}_{fuse}$, $\boldsymbol{M}_{prop}$, $\boldsymbol{M}_{duct}$, $\boldsymbol{M}_{flap}$, and $\boldsymbol{M}_{gyro}$ are the moments devolved due to to fuselage, propulsion system, duct, flaps and gyroscopic effect respectively.

There are four control flaps along the x and y axes of the body fixed frame, as shown in Fig. 13. The attitude control is performed by combination of the control flaps: two flaps (①&③) on the x- axis generate rolling moment; the others (②&④) act like an elevator to create pitching moment; and yawing motion is controlled by deflecting all the flaps (①&④) to the same rotational direction.

For a single ducted-fan UAV, a control system adopts a hierarchical structure which includes the attitude, velocity, and position loops as shown in Fig. 14. For attitude control, a model-based non-linear control approach is applied based on a sliding mode control (SMC) method with feedback linearization to cope with the non-linearity of the ducted-fan UAV model [34–36]. Proportional-integral-derivative (PID) control is designed for the position and velocity loops. The position command are fed from the task assignment and trajectory planning discussed in the previous sections as a higher-level decision making. A cascaded structure is applied with a time-scale separation for the attitude controller (Refer to [10, 37] for detailed explanation). The nonlinear adaptive controller can be designed to improve the control performance of multi-agent systems [38,39].

Fig. 15 shows the position variation of the first decoy and is clear that the desired positions are followed by the actual decoys with a negligible tolerance level. The subscript 'act' and 'des' indicates the actual and the desired values of ducted fan coordinates. Fig. 16 shows the control and state variations for a single decoy. The time histories of Euler angles, angular rates, velocities and control surfaces are shown to follow the given commands. In summary, the commands fed from the TA for the decoy mission are reasonable enough for realistic UAV models to follow under their maneuvering capabilities. The states and control inputs of the other decoys are omitted for brevity.

6. CONCLUSION

This paper proposed the task assignment for the deployment strategy of decoy systems against anti-ship missiles using auction algorithm. The cost function is calculated based on the expected signal power, calculated by the seeker and decoy signal models, along with relative distance and energy backup of the decoy. The simple kinematics is used to generate each two-dimensional motion for the ASM and the target ship. In order to verify the maneuvering capability of the decoy, the numerical simulation is conducted with three missiles and 20 decoys.

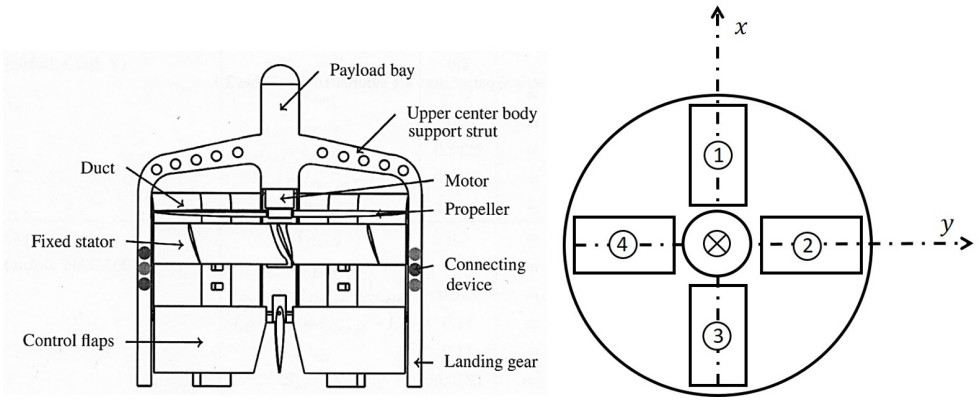

Fig. 13. A ducted-fan model and control flaps (bottom view).

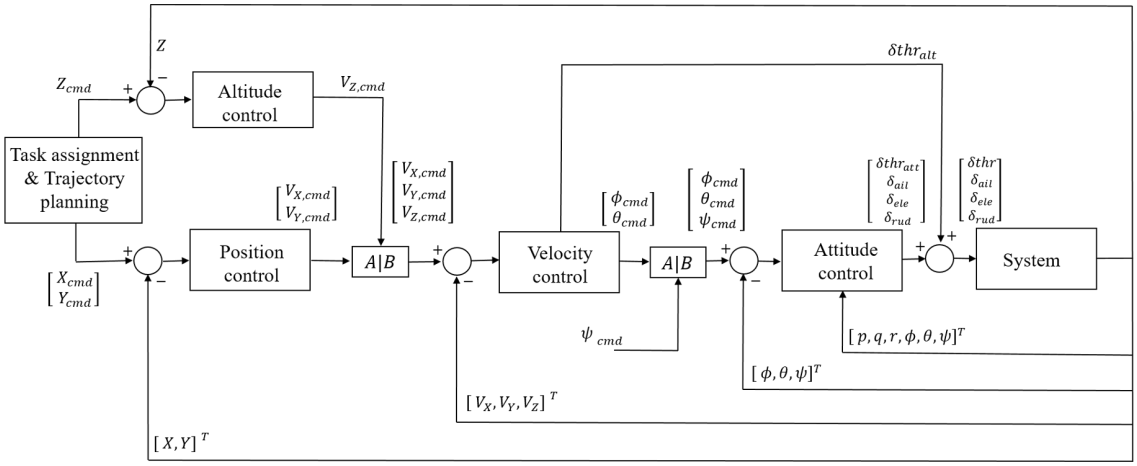

Fig. 14. Hierarchical control system structure considering TA and outer/inner loop control.

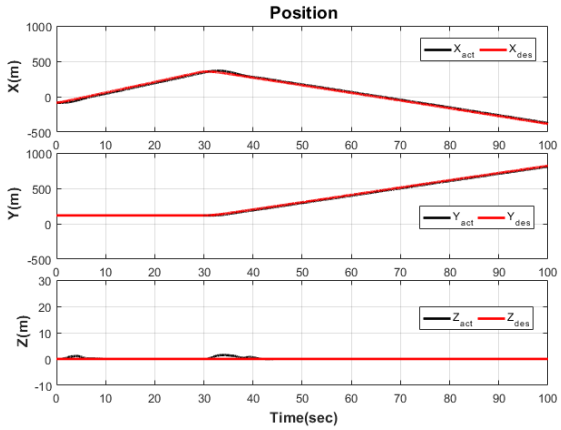

Fig. 15. Position variation of the first decoy.

To evaluate the real time response of the decoy, the nonlinear kinematics and dynamics of ducted fan model were applied. Parametric study shows that the detection radius of the ship and missile velocities were the critical factors to affect the success/failure of the mission because their response times were heavily dependent on the above two factors. This study considered the circular formation of UAVs around the ship as a precaution, and this led more fuel consumption. To overcome the limitation, additional UAVs can be added into the group; thus, the initial formation size can be increased. Possible future work can include consideration of the 3D UAV motion and jammer antenna direction based on UAV's heading. The proposed approaches in this study can be extended by adding several scenarios, uncertainties and the requirements for the applications to intruder tracking, surveillance and rescue missions.

REFERENCES

[1] K. Sakurama, Y. Kosaka,and S.-I. Nishida, "Formation control of swarm robots with multiple proximity distance sensors," *International Journal of Control, Automation and Systems*, vol. 16, no. 1, pp. 16-26, 2018.

[2] R. V. Cowlagi, J. P. Sperry, and J. C. Griffin, "Unmanned aerial vehicle trajectory optimization for executing intelligent tasks," *Journal of Guidance, Control and Dynamics*, vol. 41, no. 6, pp. 1389-1396, 2018.

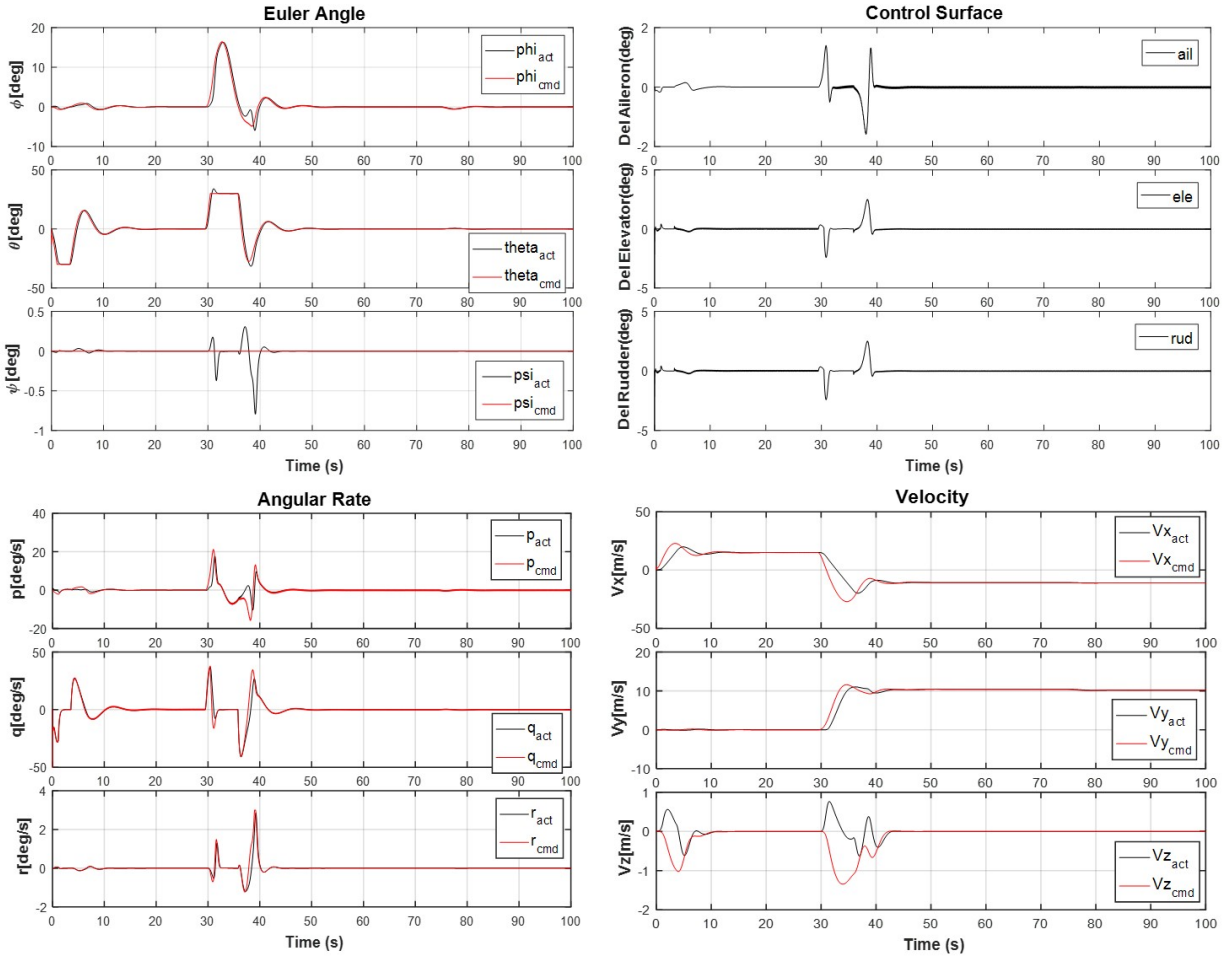

Fig. 16. Control and State variations for a single ducted-fan UAV.

[3] H.-S. Shin and P. Segui-Gasco, "UAV Swarms: Decision-making paradigms," *Encyclopedia of Aerospace Engineering, John Wiley and Sons Ltd*, pp. 1-13, 2014. DOI: 10.1002/9780470686652.eae273

[4] L. Xue, C. Sun, and D. C. Wunsch II, "A game-theoretical approach for a finite-time consensus of second-order multi-agent system," *International Journal of Control, Automation and Systems*, vol. 17, no. 5, pp. 1071-1083, 2019.

[5] X. Hu, J. Cheng, and H. Luo, "Task assignment for multi-UAV under severe uncertainty by using stochastic multi-criteria acceptability analysiss," *Mathematical Problems in Engineering*, Hindawi Publishing Corporation, Article ID 249825, 2004.

[6] B. P. Gerkey and M. J. Mataric, "A formal analysis and taxonomy of task allocation in multi-robot systems," *International Journal of Robotics Research*, vol. 23, no. 9, pp. 939-954, 2004.

[7] I. Jang, H. Shin, and A. Tsourdos, "Game-theoretical approach to heterogeneous multi-robot task assignment problem with minimum work-load requirements," *Workshop on Research, Education and Development of Unmanned Aerial Systems (RED-UAS)*, pp. 156-161, 2017.

[8] S. Yoon, H. Do, and J. Kim, "Collaborative mission and route planning of multi-vehicle systems for autonomous search in marine environment," *International Journal of Control, Automation and Systems*, vol. 18, no. 3, pp. 546-555, 2020.

[9] S. Koo, S. Kim, J. Suk, Y. Kim, and J. Shin, "Improvement of shipboard landing performance of xed-wing uav using model predictive control," *International Journal of Control, Automation and Systems*, vol. 16, no. 6, pp. 2697-2708, 2018.

[10] J. Jeong, B. Yu, T. Kim, S. Kim, J. Suk, and H. Oh, "Maritime application of ducted-fan flight array system: Decoy for anti-ship missile," *Workshop on Research, Education and Development of Unmanned Aerial Systems (RED-UAS)*, pp. 72-77, 2017.

[11] D. Kim and C.-K. Ryoo, "Defense strategy against multiple anti-ship missiles," *Proc. of ICROS-SICE International Joint Conference,* Fukuoka International Congress Center, Japan, pp. 3635-3639, 2009.

[12] H.-R. Park and I.-H. Whang, "An effective target selection algorithm for ASM (anti-ship missile)," *Proc. of SICE-ICASE International Joint Conference*, pp. 2930-2934, 2006, Busan, Korea.

[13] J.-P. Dong, J.-G. Sun, Y. Guo, S.-M. Song, "Guidance laws against towed decoy based on adaptive back-stepping sliding mode and anti-saturation methods," *International Journal of Control, Automation and Systems*, vol. 16, no. 4, pp. 1724-1735, 2018.

[14] W. J. Kerins, "Analysis of towed decoys," *IEEE Transactions on Aerospace and Electronic Systems*, vol. 29, no. 4, pp. 122-1227, 1993.

[15] Y. Zhou, "Correlation parameters simulation for towed radar active decoy," *Proc. of International Conference on Computer Distributed Control and Intelligent Environmental Monitoring*, Hunan, China, pp. 214-217, 2012.

[16] T.-H. Tan, *Effectiveness of Off-board Active Decoys Against Anti-Shipping Missiles*, Master's thesis, Naval Post-gradate school, Manterey, California, USA, 1996.

[17] V. Arthur and M. Gerrit, "Missile avoidance maneuvres with simultaneous decoy deployment," *Proc. of AIAA Guidance, Navigation, and Control Conference*, Chicago, Illinois, Aug. 2009.

[18] R. Ragesh, A. Ratnoo, and D. Ghose, "Decoy launch envelopes for survivability in an interceptor-target engagement," *Journal of Guidance, Control, and Dynamics*, vol. 39, no. 3, pp. 667-676, 2016.

[19] C. Zhai, F. He, Y. Hong, L. Wang, and Y. Yao, "Coverage-based interception algorithm of multiple interceptors against the target involving decoys," *Journal of Guidance, Control, and Dynamics*, vol. 39, no. 7, pp. 1647-1653, 2016.

[20] J. Qin and X. Wu, "Modeling and simulation on the earliest launch time of ship-to-air missile of warship formation in cooperative air-defense," *Proc. of IEEE Advanced Information Management, Communicates, Electronic and Automation Control Conference (IMCEC),*, Xi'an, China, pp. 375-379, 2016.

[21] B. Pang, Y. Song, C. Zhang, H. Wang, and R. Yang, "Autonomous task allocation in a swarm of foraging robots: An approach based on response threshold sigmoid model," *International Journal of Control, Automation and Systems*, vol. 17, no. 4, pp. 1031-1040, 2019.

[22] D.-W. Yoo, C.-H. Lee, M.-J. Tahk, and H.-L. Choi, "Optimal resource management algorithm for unmanned aerial vehicle missions in hostile territories," *Proc. of the Institution of Mechanical Engineers, Part G: Journal of Aerospace Engineering*, vol. 228, no. 12, pp. 2157-2167, 2014.

[23] Z. Jia, J. Yu, X. Ai, X. Xu, and D. Yang, "Cooperative multiple task assignment problem with stochastic velocities and time windows for heterogeneous unmanned aerial vehicles using a genetic algorithm," *Aerospace Science and Technology*, vol. 76, pp. 112-125, 2018.

[24] K. Alaa, H. Ahmed, and E. Ahmed, "Multi-robot task allocation: A review of the state-of-the-art," *Proc. of Cooperative Robots and Sensor Networks*, Springer International Publishing, pp. 31-51, 2015.

[25] K. A. Ghamry, M. A. Kamel, and Y. Zhang, "Multiple UAVs in forest fire fighting mission using particle swarm optimization," *Proc. of International Conference on Unmanned Aircraft Systems (ICUAS)*, Miami, FL, USA, pp. 1404-1409, 2017.

[26] A. K. Pamosoaji, M. Piao, and K.-S. Hong, "PSO-based minimum-time motion planning for multiple vehicles under acceleration and velocity limitations," *International Journal of Control, Automation and Systems*, vol. 17, no. 10, pp. 2610-2623, 2019.

[27] I. Maza, F. Caballero, J. Capitán, J. R. Martínez-de-Dios, and A. Ollero, "Simulations of repeat jamming against anti-ship missile seekers which use doppler beam sharpening modes," *International Journal of Control, Automation and Systems*, vol. 16, no. 6, pp. 2727-2732, 2011.

[28] Z. Tang and C. Li, "Distributed event-triggered containment control for discrete-time multi-agent systems," *International Journal of Control, Automation and Systems*, vol. 16, no. 6, pp. 2727-2732, 2018.

[29] Z. Tang, "Event-triggered consensus of linear discrete-time multi-agent systems with time-varying topology," *International Journal of Control, Automation and Systems*, vol. 16, no. 3. pp. 1179-1185, 2018.

[30] A. M. Khamis, A. Hussein, and A. M. Elmogy, "Multi-robot task allocation: A review of the state-of-the-art," *Studies in Computational Intelligence*, vol. 604, pp. 31-51, 2015.

[31] B. Oh, J. Jeong, J. Suk, and S. Kim, "Design of a control system for an organic flight array based on a neural network controller," *International Journal of Aerospace Engineering*, vol. 2018, Article ID 1250908, pp. 1-11, 2018.

[32] E. N. Johnson and M. A. Turbe, "Modelling, control, and flight testing of a small-ducted fan aircraft," *Journal of Guidance, Control, and Dynamics*, vol. 29, no. 4, pp. 769-779, 2006.

[33] J. M. Pflimlin, P. Soueres, and T. Hamel, "Position control of a ducted fan VTOL UAV in crosswind," *International Journal of Control*, vol. 80, no. 5, pp. 666-683, 2007.

[34] T. Jiang , T. Song, and D. Lin, "Integral sliding mode based control for quadrotors with disturbances: Simulations and experiments," *International Journal of Control, Automation and Systems*, vol. 17, no. 8, pp. 1987-1998, 2019.

[35] Y. Shtessel, J. Buffington, and S. Banda, "Multiple time scale flight control using reconfigurable sliding modes," *Journal of Guidance, Control, and Dynamics*, vol. 22 no. 6, pp. 87-883, 1999.

[36] C. I. Ahn, Y. Kim, and H. Kim, "Adaptive sliding mode controller design for fault tolerant flight control system," *Proc. of AIAA Guidance, Navigation, and Control Conference and Exhibit, Guidance, Navigation, and Control and Co-located Conferences*, Keystone, Colorado, 2006.

[37] J. Jeong, *Dynamics and Control of Ducted-fan Flight Array System*, Ph.D. thesis, Chungnam National University, Korea, 2017.

[38] S. Islam and N. I. Xiros, "Robust asymptotic and finite-time tracking for second-order nonlinear multi-agent autonomous systems," *International Journal of Control, Automation and Systems*, vol. 17, no. 12, pp. 3069-3078, 2019.

[39] Z. Hou, J. Xu, G. Zhang, W. Wang, and C. Han, "Interaction Matrix Based Analysis and Asymptotic Cooperative Control of Multi-agent Systems," *International Journal of Control, Automation and Systems*, vol. 18, no. 5, pp. 1103-1115, 2020.

Dileep M V received his B.Tech. degree in electronics and communication engineering from University of Kerala, Kerala, India in 2010, an M.Tech. degree technology in astronomy and space engineering from Manipal university, Karnataka, India in 2012. He obtained a Ph.D. degree in Optimization and control, Manipal Institute of Technology, Manipal University, Karnataka, India in 2017 and now working as a Post-doc researcher, Department of Aerospace Engineering, Chungnam National University, Korea. His areas of interest are control applications for UAV path planning, decision making for unmanned systems and optimization algorithms with a focus on aerospace applications.

Beomyeol Yu received his B.Sc. and M.Sc. degrees in aerospace engineering from Chungnam National Unversity (CNU), Daejeon, Korea, in 2017 and 2019, respectively. His research interests cover dynamic modeling and control for various types of unmanned aerial vehicles, neural networks, reinforcement learning, cooperative aerial transportation, and embedded system implementations.

Seungkeun Kim received his B.Sc. degree in mechanical and aerospace engineering from Seoul National University (SNU), Seoul, Korea, in 2002, and then acquired a Ph.D. degree from SNU in 2008. He is currently a professor at the Department of Aerospace Engineering, Chungnam National University, Korea. He was an associate professor and an assistant professor at the same university from 2012 to 2020. Previously, he was a research fellow and a lecturer at Cranfield University, United Kingdom from 2008 to 2012. He is interested in micro aerospace systems, aircraft guidance and control, estimation, sensor fusion, fault diagnosis, fault tolerant control, and decision making for autonomous systems.

Hyondong Oh received his B.Sc. and M.Sc. degrees in aerospace engineering from Korea Advanced Institute of Science and Technology (KAIST), Korea, in 2004 and 2010, respectively, and then he acquired a Ph.D. degree on autonomous surveillance and target tracking guidance using multiple UAVs from Cranfield University, United Kingdom, in 2013. He worked as a lecturer in autonomous unmanned vehicles at Loughborough University, United Kingdom in 2014-2016. He is currently an associate professor at the School of Mechanical, Aerospace and Nuclear Engineering, Ulsan National Institute of Science and Technology (UNIST), Korea. His research interests cover autonomy and decision making, cooperative control and path planning, nonlinear guidance and control, estimation and sensor/information fusion for unmanned systems.